

---

---

OPTICAL  
PROPERTIES

---

---

# Aerosol Synthesis of Highly Dispersed $Y_3Al_5O_{12}:Ce^{3+}$ Phosphor with Intense Photoluminescence

Kh. A. Abdullin<sup>a,\*</sup>, A. E. Kemel'bekova<sup>b</sup>, V. M. Lisitsyn<sup>c</sup>, D. M. Mukhamedshina<sup>b</sup>,  
R. R. Nemkaeva<sup>a</sup>, and A. T. Tulegenova<sup>a</sup>

<sup>a</sup>National Nanotechnology Laboratory of Open Type (NNLOT),  
Al-Farabi Kazakh National University, Almaty, 050040 Kazakhstan

<sup>b</sup>Satbayev University, Institute of Physics and Technology, Almaty, 050013 Kazakhstan

<sup>c</sup>National Research Polytechnic University, Tomsk, 634050 Russia

\*e-mail: kh.abdullin@physics.kz

Received June 3, 2019; revised June 3, 2019; accepted June 4, 2019

**Abstract**—A simple method of pyrolysis of an aerosol solution of yttrium, aluminum, and cerium nitrates with the addition of urea or citric acid, followed by brief annealing, is developed to obtain a highly dispersed aluminum–yttrium garnet powder that demonstrates intense photoluminescence in the visible light region. Characterization of the synthesized samples (photoluminescence spectra, X-ray diffraction analysis, Raman spectra) showed that intense photoluminescence is achieved only in a narrow window of process conditions, namely, the concentration of nitrate solution and the concentration of citric acid or urea. The photoluminescence intensity increases upon annealing synchronously with an increase in the crystallite size, which, along with the optimal cerium concentration (~0.5 at %), is a determining factor for obtaining high-quality samples. The synthesized powders had intense photoluminescence and high optical perfection, as evidenced by the observation of whispering gallery modes.

**Keywords:** aerosol synthesis, highly dispersed YAG:Ce<sup>3+</sup>, whispering gallery modes

**DOI:** 10.1134/S1063783419100020

## 1. INTRODUCTION

Energy efficient white light-emitting diodes (WLEDs) are now widely used as solid-state optical sources in various fields, for example, general lighting, automotive lighting, display screen backlight sources, etc. [1, 2]. White light can be obtained using various combinations of LEDs and phosphors. Currently, InGaN–AlGaN blue LEDs and a system of yellow phosphors are used as a commercial WLEDs, because of the simplicity of construction, low cost, and an excellent color rendering index (CRI) [3].

Phosphor  $Y_3Al_5O_{12}:Ce^{3+}$  (YAG:Ce<sup>3+</sup>) is one of the optimal phosphor materials for WLEDs due to its high quantum efficiency, high refractive index, strength, and excellent chemical and thermal stability [3, 4]. YAG:Ce<sup>3+</sup> phosphors are conventionally synthesized by solid-phase reaction with prolonged annealing at high temperature (>1500°C). To obtain a powder useful for WLED manufacturing, subsequent grinding is necessary, which can cause contamination of the material, because YAG:Ce<sup>3+</sup> is a rather hard material (approximately 8.5 by the Mohs scale).

To overcome the above disadvantages, various methods are being developed for the production of

pure and homogeneous highly dispersed YAG:Ce<sup>3+</sup> phosphors, such as controlled glass crystallization [5], flame pyrolysis [6], sol–gel process [7, 8], laser ablation [9], hydrothermal synthesis using microwave radiation [10], coprecipitation of the corresponding salts from solutions [11], and aerosol pyrolysis [12].

Upon synthesizing highly dispersed YAG:Ce<sup>3+</sup> powders with intense photoluminescence (PL), the problem is to achieve high crystallinity of the material and prevent the loss of cerium. Therefore, highly dispersed YAG:Ce<sup>3+</sup> often has an almost white color and weak photoluminescence, the intensity of which is low compared with that of commercial yellow phosphors. In this work, highly dispersed YAG:Ce<sup>3+</sup> was obtained by simple aerosol pyrolysis followed by short-term annealing; the photoluminescence intensity of the samples synthesized under optimal conditions is ~40% of the photoluminescence of the YAG:Ce<sup>3+</sup> phosphor of industrial quality.

## 2. EXPERIMENTAL

The working solution was prepared at a molar ratio of yttrium to aluminum of 3:5 by dissolving yttrium nitrate ( $Y(NO_3)_3 \cdot 6H_2O$ , Sigma Aldrich), aluminum

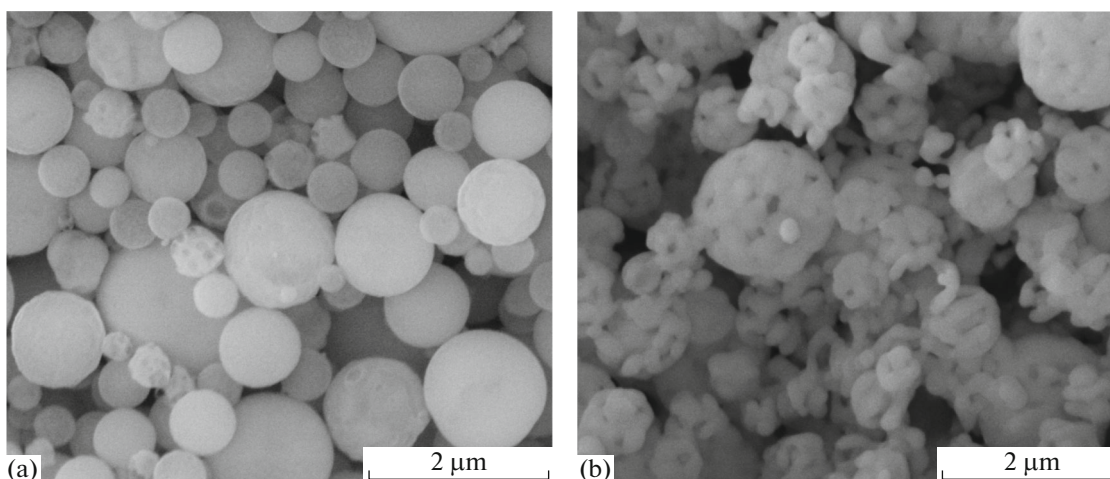
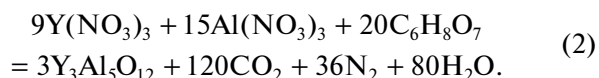
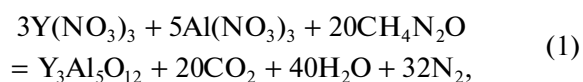


Fig. 1. SEM images of the sample (a) after synthesis at 800°C and (b) after annealing at 1550°C.

nitrate ( $Al(NO_3)_3 \cdot 9H_2O$ , Sigma Aldrich), and cerium nitrate ( $Ce(NO_3)_3 \cdot 6H_2O$ , Sigma Aldrich) in deionized water. The concentration of the solution in terms of cerium was 0.5 at %. To neutralize nitric acid, which is released during the thermal decomposition of yttrium and aluminum nitrates, urea ( $NH_2CONH_2$ ) or citric acid ( $C_6H_8O_7$ ) was added to the working solution. The following reactions preventing the release of acid may occur:



Powders were synthesized by aerosol pyrolysis. The piezoelectric ultrasonic generator produced aerosol from the working solution; the aerosol was transferred by the air flow generated by the compressor into a vertical tube furnace heated to 800°C. Aerosol pyrolysis occurred in the hot zone of the furnace. Oxide particles were captured by a cylindrical electrostatic filter at the exit of the furnace and were easily separated from filter walls after synthesis.

The morphology of the samples was investigated using a Quanta 3D 200i FEI scanning electron microscope (SEM). The photoluminescence spectra of the  $YAG:Ce^{3+}$  samples were measured at room temperature using a Cary Eclipse fluorescence spectrometer (Agilent) under excitation with a pulsed xenon lamp. Raman spectra were recorded at room temperature using a Solver Spectrum spectrometer (NT-MDT) with laser excitation at 633 nm; the same spectrometer was used to study microphotoluminescence ( $\mu$ -PL) at room temperature. The microphotoluminescence spectra were excited by a 473-nm laser spot diameter of  $\sim 2 \mu m$  through a 100-fold Mitutoyo lens. X-ray dif-

fraction (XRD) studies were performed using a Mini-Flex Rigaku diffractometer with  $CuK\alpha$  radiation.

### 3. RESULTS AND DISCUSSION

Typical SEM images of the powder obtained by pyrolysis at 800°C of a solution with citric acid are shown in Fig. 1a. Figure 1b shows an SEM image of the same sample after annealing in air at 1300°C for 30 min. The powder is highly dispersed, with the particle sizes less than 2  $\mu m$ ; the particles consist of smaller ( $\sim 100$  nm) particles. Similar results were obtained in the synthesis using solutions with urea (not shown).

The X-ray diffraction patterns of samples subjected to isochronous (30 min) annealing in the temperature range from 800 to 1550°C are presented in Fig. 2. In all experiments on annealing, the heating rate was 10°C/min. The broad peaks in the diffraction pattern of the sample immediately after synthesis (the lower curve in Fig. 2) indicate that oxides formed by the pyrolysis of nitrates are present in the synthesized samples in a nanocrystalline or amorphous state. The hexagonal lattice of yttrium–aluminum oxide  $YAlO_3$  is formed at an annealing temperature of 900°C (Fig. 2); the X-ray pattern is consistent with the reference one for  $YAlO_3$  (PDF Card no. 00-054-0621).

Since cerium oxide has a high melting point, preventing the formation of large particles of the  $CeO_2$  phase is a significant problem. Otherwise, the concentration of  $Ce^{3+}$  impurity atoms dissolved in the YAG matrix is low, and, accordingly, the photoluminescence intensity is low.

Weak peaks of cubic  $Y_3Al_5O_{12}$  garnet (PDF Card no. 00-033-0040) appear after annealing at 900°C. The garnet phase becomes dominant in the samples annealed above 1000°C. The XRD peaks at angles of

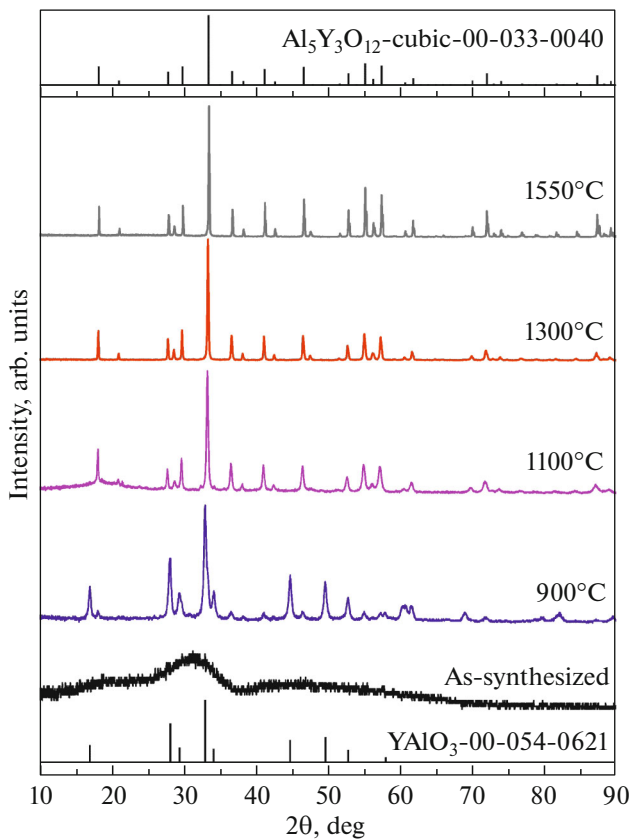


**Fig. 2.** X-ray diffraction patterns of the samples obtained by pyrolysis at 800°C, followed by annealing in the air for 30 min, at temperatures up to 1550°C.

16.8°, 44.8°, 49.6°, and 57.9°, related to the hexagonal phase of YAlO<sub>3</sub>, disappear after annealing at 1000°C.

The average crystallite size  $D$  was estimated from X-ray diffraction patterns using a MiniFlex Rigaku diffractometer processing software based on the Williamson–Hall method [13]. The crystallite size  $D$  was also estimated by the Scherrer equation,  $D = (0.89\lambda)/(\beta \cos\theta)$ , where  $\beta$  is the full width at half maximum (FWHM) of the X-ray diffraction line observed in experimental X-ray spectra at angles  $2\theta$ , and  $\lambda = 0.1540$  nm is the  $K_{\alpha}$  wavelength of the X-ray copper line. The graphs of  $D$  values obtained by both methods, depending on the temperature of isochronous (30 min) annealing, are shown in Fig. 3. The results obtained by both methods give similar values. The average size of crystallites increases from ~15 to ~90 nm with an increase in the annealing temperature from 800 to 1550°C. At the same time, the lattice deformation decreased from 0.26 to 0.04%.

The Raman spectra of a reference sample, that is, an industrial YAG:Ce<sup>3+</sup> phosphor synthesized in Platan (Moscow region, Russia), which is referred to as Ref-YAG:Ce<sup>3+</sup> (spectrum 1), and a powder obtained by pyrolysis of a solution with citric acid and subse-

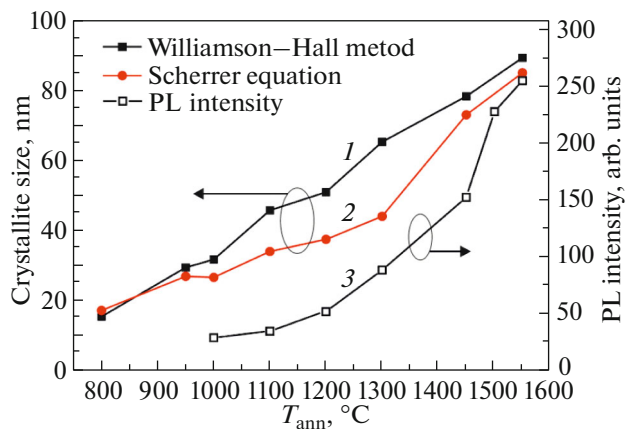


**Fig. 3.** Average crystallite size for YAG samples, determined from XRD data by (1) the Williamson–Hall method and (2) the Scherrer equation. (3) Dependence of the photoluminescence intensity on the annealing temperature for the same samples.

quent annealing at 1550°C for 30 min are presented in Fig. 4. All observed bands at 163, 218, 263, 342, 375, and 404 cm<sup>-1</sup> are characteristic of YAG. They can be compared with the well-known Raman bands of YAG at 160, 218, 259, 340, 371, and 401 cm<sup>-1</sup> [14]; the positions of the Raman bands differ little from those for single-crystal samples.

Thus, highly dispersed single-phase YAG powders can be obtained by short-term (~30 min) annealing at temperatures above 1000°C. The presence of one phase in YAG:Ce<sup>3+</sup> samples is a necessary condition for achieving high photoluminescence efficiency [1]. In addition to high crystallinity, it is also essential to maintain the impurity concentration of cerium ions Ce<sup>3+</sup> at an optimum level and prevent the formation of a cerium oxide phase.

The photoluminescence properties of the YAG:Ce<sup>3+</sup> samples were investigated depending on the concentration of citric acid or urea in the working solution and the temperature of the subsequent heat treatment. It was found that high photoluminescence intensity in single-phase YAG samples is achieved only in a narrow range of concentrations of the working solution. Nitric acid formed during pyrolysis decreases the concentration of cerium due to acid etching of the sample. The presence of acid also diminishes the crystallite size, which prevents the achievement of intense photoluminescence.

The photoluminescence intensity after annealing remained low with the addition of urea and citric acid in stoichiometric amounts corresponding to reactions (1) and (2), and a significant increase in the photoluminescence intensity was observed with an increase in the concentration of citric acid (or urea). The maximum intensity was reached when the level of citric acid or urea exceeded the stoichiometric amount three

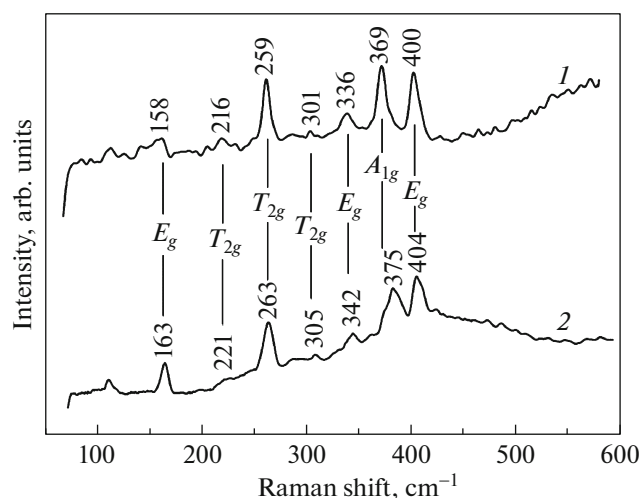


**Fig. 4.** Raman spectra of (1) the Ref-YAG:Ce<sup>3+</sup> sample and (2) the sample synthesized at 800°C, followed by annealing at 1550°C for 30 min.

times. A further increase in the amount of urea or citric acid in the working solution resulted in small YAG crystallites and caused a decrease in the intensity of the photoluminescence. For the same reason, low photoluminescence intensity was observed when a solution with a yttrium concentration of less than 0.1 M was used.

The dependence of the photoluminescence intensity on the annealing temperature for samples grown using a working solution with a threefold excess over the stoichiometric amount of citric acid is shown in Fig. 3 (curve 3). Noticeable photoluminescence appeared only after annealing at 1000°C, when  $\text{YAlO}_3$  oxide disappears, and the phase of the YAG garnet becomes dominant (Fig. 2). The photoluminescence intensity increases in the annealing temperature range from 1000 to 1550°C simultaneously with an increase in the crystallite size (Fig. 3).

The samples obtained after synthesis using citric acid was a black powder due to the presence of a small amount of carbon black, while after synthesis using urea, the powder was white. After high-temperature annealing, the photoluminescence intensity in the samples obtained with citric acid was always significantly higher than that for samples synthesized with urea. This may be because the presence of carbon black on the surface of the particles blocks the agglomeration of cerium in the cerium oxide phase due to the creation of reducing conditions, thereby maintaining the concentration of dissolved cerium in the YAG samples.

Figure 5 shows the comparison of the photoluminescence spectra of Ref-YAG:Ce<sup>3+</sup> phosphor (spectrum 1) and YAG:Ce<sup>3+</sup> samples synthesized using solutions with citric acid (spectrum 2) and urea (spec-

trum 3) by pyrolysis at 800°C, followed by annealing in air at 1550°C for 30 min. The energy of the photoluminescence band maximum coincides well with the well-known literature data for YAG:Ce<sup>3+</sup> [5, 15, 16]. The photoluminescence excitation spectra consist of two bands with peaks at ~340 and 450 nm (Fig. 5a), which is characteristic of YAG:Ce<sup>3+</sup>.

The resulting phosphor YAG:Ce<sup>3+</sup> after annealing at 1550°C was a yellow powder; its color was slightly less intense than that of the Ref-YAG:Ce<sup>3+</sup> sample. The integrated photoluminescence intensity of the sample was  $(40 \pm 2)\%$  of the intensity of the Ref-YAG:Ce<sup>3+</sup> sample.

Spectra 1 and 2 from Fig. 5a can be decomposed into two Gaussians (Fig. 5b). The photoluminescence spectrum of the Ref-YAG:Ce<sup>3+</sup> sample consists of peaks at 530 nm (peak I) and 574 nm (peak II); the spectrum of the YAG:Ce<sup>3+</sup> sample consists of peaks at 524 nm (I) and 563 nm (II). The presence of two peaks is characteristic of  $5d^1-4f^1$  ( ${}^2F_{5/2}$ ) and  $5d^1-4f^1$  ( ${}^2F_{7/2}$ ) transitions of the Ce<sup>3+</sup> ion. The distance between the components in the photoluminescence spectrum also corresponds to the published data [17] on the  $4f^05d^1 \rightarrow 4f^1$  transitions of the Ce<sup>3+</sup> ion. The  $4f^1$  ground state configuration is divided into two sublevels,  ${}^2F_{5/20}$  and  ${}^2F_{7/2}$ , and these two sublevels are separated by approximately 2000  $\text{cm}^{-1}$  due to the spin-orbit coupling [18]. In our case, the distance between the photoluminescence bands with maxima at 2.20 and 2.37 eV is  $\sim 1400 \text{ cm}^{-1}$ , which is fairly close to the literature data. Upon excitation at 450 nm, the Ref-YAG:Ce<sup>3+</sup> sample (Fig. 5a, spectrum 1) showed chromaticity coordinates  $X = 0.419$ ,  $Y = 0.553$ , and  $Z = 0.028$ , and the YAG:Ce<sup>3+</sup> sample (Fig. 5a, spectrum 2) yielded close values of  $X = 0.391$ ,  $Y = 0.570$ , and  $Z = 0.039$ .

The synthesized phosphors were also investigated by microphotoluminescence at room temperature. The position of the microphotoluminescence peak practically coincides with the position of the photoluminescence spectrum excited at 450 nm. However, some regions of the sample demonstrate the modulation of the microphotoluminescence spectrum (Fig. 6). These oscillations can be caused either by optical interference in a Fabry-Pérot resonator or by whispering gallery modes [19, 20].

Using a simple ratio for resonant wavelengths of  $2nL \cos\theta = N\lambda$ , where  $n$  is the refractive index,  $L$  is the length of the resonator,  $\theta$  is the angle of incidence,  $N$  is an integer,  $\lambda$  is wavelength, we can estimate the size  $L$  of the structures in which interference takes place. The excellent coincidence of the positions of the maxima in the microphotoluminescence spectra with the above equation was obtained with  $n = 1.886$ ,  $L = 2.92 \mu\text{m}$ , and  $N = 16-22$  for small YAG:Ce<sup>3+</sup> particles

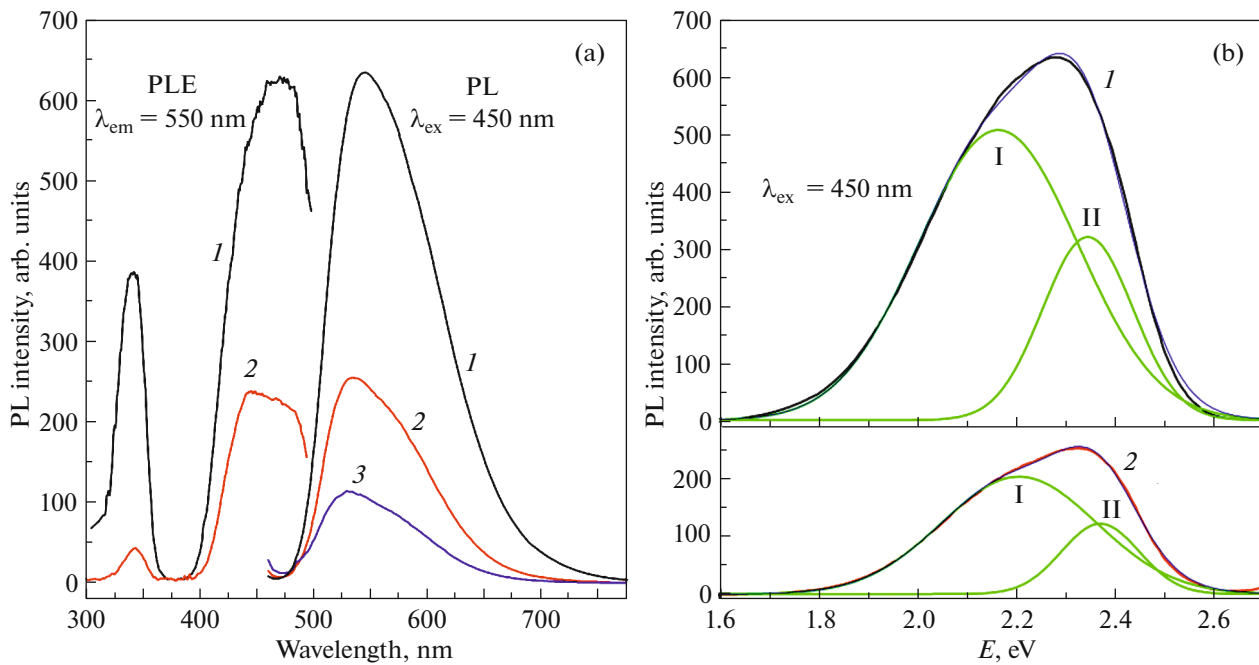


**Fig. 5.** (a) Spectra of photoluminescence excitation and photoluminescence of (1) Ref-YAG:Ce<sup>3+</sup> and the samples obtained by pyrolysis of the precursor solution with (2) citric acid and (3) urea. (b) Decomposition of the photoluminescence spectra shown in Fig. 5a into two Gaussians; energy is plotted along the x axis.

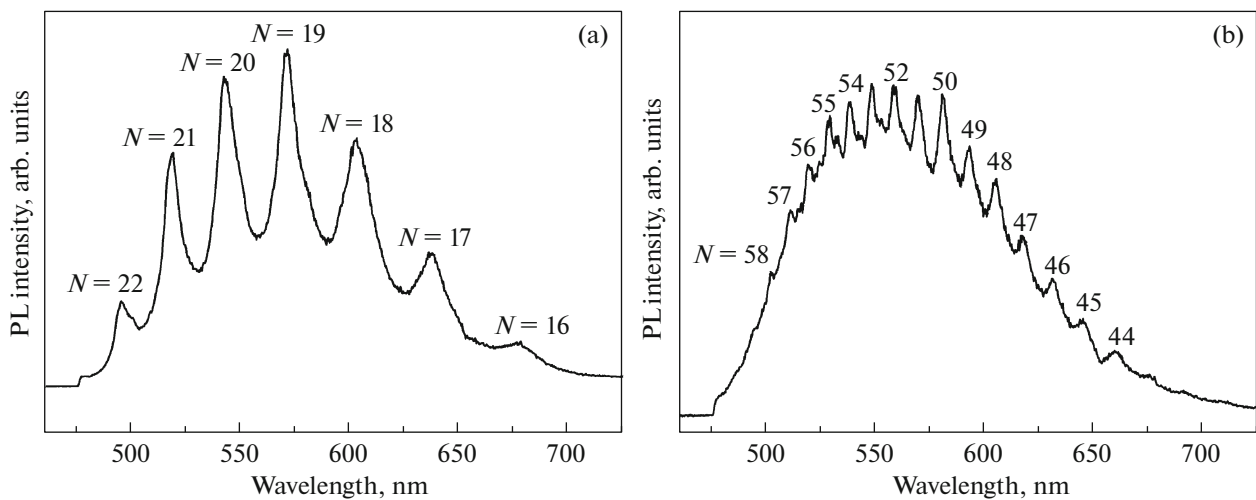


**Fig. 6.** Microphotoluminescence spectra of (a) small and (b) large YAG:Ce<sup>3+</sup> particles.

(Fig. 6a) and  $L = 7.80 \mu\text{m}$  and  $N = 44\text{--}58$  for large YAG:Ce<sup>3+</sup> particles (Fig. 6b).

According to SEM analysis, particles with sizes larger than  $2\text{--}4 \mu\text{m}$  are not observed; in addition, the size of the excitation region is approximately  $2 \mu\text{m}$ . Consequently, the observed microphotoluminescence spectra (Figs. 6a and 6b) cannot be explained by the Fabry–Pérot resonance and must be attributed to the whispering gallery modes for round particles with an

average size of  $\sim 0.9$  and  $\sim 2.5 \mu\text{m}$ , respectively. These values are in good agreement with the observed particle sizes of the YAG:Ce<sup>3+</sup> powder. Thus, the observed modulation of the microphotoluminescence spectrum in the synthesized phosphor can be explained by the circular resonances of whispering gallery modes (WGM) and, to our knowledge, these modes have not previously been observed in YAG:Ce<sup>3+</sup> microcrystals. It can be concluded that the synthesized samples have

high optical characteristics. The WGM interference effect can be useful for various applications, including sensorics and photonics; WGM optical microresonators are very promising for use in optoelectronic and biological surface optical sensors [20].

#### 4. CONCLUSIONS

A simple method of pyrolysis of aerosol was used for the synthesis of highly dispersed  $YAG:Ce^{3+}$  powder with intense photoluminescence. Optimal conditions were determined for maintaining the concentration of cerium, achieving high crystallinity during short-term annealing, and obtaining intense photoluminescence. After synthesis at  $800^\circ C$ , the material has an amorphous structure; upon annealing, the  $YAlO_3$  oxide phase is first formed, and at temperatures above  $1000^\circ C$ , the garnet  $Y_3Al_5O_{12}$  structure is observed. A relationship close to linear was found between the photoluminescence intensity and the crystallite size. The intensity of the photoluminescence spectra of  $Y_3Al_5O_{12}$  depends on the total concentration of the working solution and the amount of citric acid (or urea). When using citric acid, carbon black is present in the samples after synthesis, which creates reducing conditions during subsequent annealing and prevents the loss of cerium. Observation of the whispering gallery modes indicates a high optical quality of the synthesized material.

#### FUNDING

This work was partially supported by the Ministry of Education and Science of the Republic of Kazakhstan, grant no. AP05130243.

#### CONFLICT OF INTERESTS

The authors declare that they have no conflicts of interest.

#### REFERENCES

1. R. Zhang, H. Lin, Y. Yu, D. Chen, J. Xu, and Y. Wang, *Laser Photon. Rev.* **8**, 15 (2013).
2. S. Nakamura, *Angew. Chem., Int. Ed.* **54**, 7770 (2015).

3. Y. Hwa Kim, N. S. M. Viswanath, S. Unithrattil, H. J. Kim, and W. B. Im, *ECS J. Solid State Sci. Technol.* **7**, R3134 (2018).
4. Y.-C. Lin, M. Karlsson, and M. Bettinelli, *Top. Curr. Chem.* **21**, 374 (2016).
5. G. He, L. Mei, L. Wang, G. Liu, and J. Li, *Cryst. Growth Des.* **11**, 5355 (2011).
6. A. Purwanto, W.-N. Wang, T. Ogi, I. W. Lenggoro, E. Tanabe, and K. Okuyama, *J. Alloys Compd.* **463**, 350 (2008).
7. S. Murai, K. Fujita, K. Iwata, and K. Tanaka, *J. Phys. Chem. C* **115**, 17676 (2011).
8. F. A. Selim, A. Khamehchi, D. Winarski, and S. Agarwal, *Opt. Mater. Express* **6**, 3704 (2016).
9. H. Koizumi, J. Watabe, S. Sugiyama, H. Hirabayashi, Y. Tokuno, H. Wada, and T. Homma, *ECS J. Solid State Sci. Technol.* **7**, R63 (2018).
10. P. Ramanujam, B. Vaidhyanathan, J. Binera, S. Ghannizadeh, Z. Zhou, and C. Spacie, *Am. Ceram. Soc.* **101**, 4864 (2018).
11. G. P. Shevchenko, E. V. Tret'yak, S. K. Rakhmanov, and G. E. Malashkevich, *Russ. J. Phys. Chem. A* **87**, 1397 (2013).
12. L. Mancic, K. Marinkovic, B. A. Marinkovic, M. Dramicanin, and O. Milosevic, *J. Eur. Ceram. Soc.* **30**, 577 (2010).
13. G. Williamson and W. Hall, *Acta Metall.* **1**, 22 (1953).
14. A. Lukowiak, R. J. Wiglusz, M. Maczka, P. Gluchowski, and W. Streck, *Chem. Phys. Lett.* **494**, 279 (2010).
15. V. M. Lisitsyn, I. P. Soshchin, Yu Yang, S. A. Stepanov, L. A. Lisitsyna, A. T. Tulegenova, and Kh. A. Abdullin, *Russ. Phys. J.* **60**, 862 (2017).
16. V. M. Lisitsyn, S. A. Stepanov, H. A. Abdullin, A. T. Tulegenova, Yangyang Ju, and V. Kolomin, *Key Eng. Mater.* **712**, 362 (2016).
17. A. B. Munoz-Garcia, Z. Barandiaran, and L. Seijo, *J. Mater. Chem.* **22**, 19888 (2012).
18. G. Blasse and A. Bril, *Appl. Phys. Lett.* **11**, 53 (1967).
19. B. Sotillo, P. Fenandez, and J. Piqueras, *J. Mater. Chem. C* **3**, 10981 (2015).
20. S. A. Grudinkin, A. A. Dontsov, N. A. Feoktistov, M. A. Baranov, K. V. Bogdanov, N. S. Averkiev, and V. G. Golubev, *Semiconductors* **49**, 1369 (2015).

*Translated by O. Zhukova*